

Efficient First-Principles Framework for Overdamped Phonon Dynamics and Anharmonic Electron-Phonon Coupling in Superionic Materials

Yuxuan Wang,¹ Marios Zacharias,^{2,*} Xiao Zhang,¹ Nick Pant,^{1,3,4}
Jacky Even,² Pierre F. P. Poudeu,¹ and Emmanouil Kioupakis^{1,†}

¹*Department of Materials Science and Engineering,*

University of Michigan, Ann Arbor, Michigan 48109, USA

²*Univ Rennes, INSA Rennes, CNRS, Institut FOTON - UMR 6082, F-35000 Rennes, France*

³*Applied Physics Program, University of Michigan, Ann Arbor, Michigan 48109, USA*

⁴*Oden Institute for Computational Engineering and Sciences,
The University of Texas at Austin, Austin, Texas 78712, USA*

(Dated: February 12, 2025)

Relying on the anharmonic special displacement method, we introduce an *ab initio* quasistatic polymorphous framework to describe local disorder, anharmonicity, and electron-phonon coupling in superionic conductors. Using the example of cubic Cu₂Se, we show that positional polymorphism yields extremely overdamped anharmonic vibrations while preserving transverse acoustic phonons, consistent with experiments. We also demonstrate well-defined electronic band structures with large band gap openings due to polymorphism of 1.0 eV and calculate anharmonic electron-phonon renormalization, yielding band gap narrowing with increasing temperature in agreement with previous measurements. Our approach opens the way for efficient *ab initio* electronic structure calculations in superionic crystals to elucidate their compelling high figure-of-merit.

Copper chalcogenides Cu₂(Se, S, Te) and related compounds have recently attracted significant attention for their unique properties and potential in thermoelectric applications [1–11], achieving a remarkable figure-of-merit (zT) above 2, compared to typical values around 1 [12, 13]. The high-temperature phase of these materials is characterized by a cubic superionic structure, featuring a disordered arrangement of Cu cations [9, 14–23]. The specific transition temperature is influenced by the degree of Cu deficiency, x , which can stabilize the cubic phase of Cu_{2- x} Se even at room temperature [14–16].

It has been proposed that, similar to liquids, superionic diffusion of Cu ions in Cu₂Se suppresses phonon modes, while the electron behavior remains consistent with crystalline semiconductors [2]. This Phonon-Liquid Electron-Crystal phenomenon has been challenged in Ref. [7], suggesting that the timescales of Cu hopping are too slow to suppress transverse acoustic phonons. The high zT has been attributed to anharmonic lattice dynamics rather than liquid-like ionic diffusion, highlighting the need for a deeper understanding of the interplay between ionic disorder and lattice vibrations in superionic conductors.

Molecular dynamics (MD) simulations [24–26] have made excellent progress in describing vibrational properties, including the low thermal conductivity. However, these simulations do not effectively distinguish between the contributions of atomic disorder and thermal disorder to the overall vibrational behavior, thus limiting their ability to fully elucidate the mechanisms underlying the high zT . Alternative approaches to vibrational dynamics in superionic conductors [27] involve phonon anharmonicity calculations [28] based on the self-consistent phonon theory [29]. While these calculations capture phonon self-energy corrections at finite temperatures [28, 30–32], they

rely on the phonon quasi-particle approximation and do not account for atomic disorder. This results in substantial discrepancies with experimental measurements of the phonon density of states (PDOS) [5, 7].

The positions of Cu atoms also impact the electronic properties, leading to, for example, significant band gap changes. Semilocal density functional theory (DFT) calculations [33, 34] predict a semi-metallic behavior in Cu₂Se when using a simulation cell with atoms at their high-symmetry positions [35–37]. Improved treatments of exchange or correlation using hybrid [38, 39] or the modified Becke-Johnson [40, 41] functionals open a band gap of 0.5 eV [35, 37, 42], underestimating experiments ranging from 0.8 to 1.5 eV [1, 43–45]. Using these functionals, empirical adjustments to the atomic positions and MD simulations for modeling atomic disorder can increase the gap up to 1.0 eV [37, 42, 46, 47].

In this paper, motivated by the progress of previous studies [24–27, 35–37, 42, 46, 47], we introduce a systematic method to study disorder and anharmonicity, separating their impact on phonon dynamics and electronic structure. We propose using a locally disordered structure, namely the polymorphous network [52, 53], whose atoms are fixed in positions that define a minimum on the potential energy surface. As previously shown for other strongly anharmonic materials [51–54], polymorphous networks yield significant corrections to the electronic structure and phonons compared to calculations based on the high-symmetry (monomorphous) structure.

Here, we employ the Anharmonic Special Displacement Method (ASDM) [32, 51, 55] to explore polymorphous structures, anharmonicity, and electron-phonon coupling in cubic Cu₂Se. Our calculations show that accounting for local disorder yields overdamped vibrations

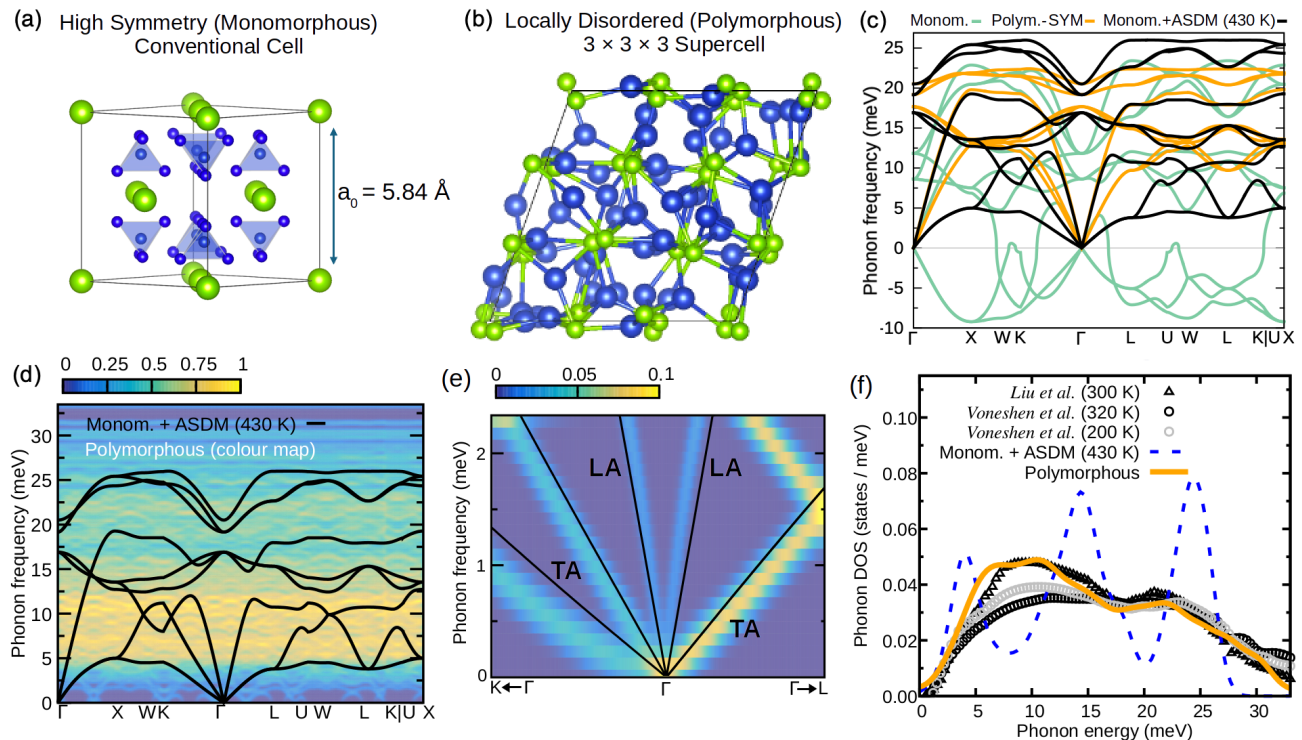


FIG. 1. (a) Conventional cell of cubic Cu_2Se , showing the high-symmetry structure (Fm-3m) with four equivalent Cu 32f site forming a tetrahedron centered at the symmetric 8c Wyckoff position [14, 48–50]. The lattice parameter is set to the $a_0 = 5.84 \text{ \AA}$ [48]. (b) Polymorphous structure of cubic Cu_2Se in a $3 \times 3 \times 3$ supercell. (c) Harmonic phonon dispersion of cubic Cu_2Se calculated for the monomorphous (green) and the $3 \times 3 \times 3$ polymorphous structure (orange). Interatomic force constants calculated for the polymorphous structure are symmetrized based on the monomorphous crystal’s symmetries. The anharmonic phonon dispersion at 430 K calculated via the ASDM is shown as black. (d) Phonon spectral function (color map) calculated for the polymorphous structure without enforcing symmetries and using phonon unfolding [51] for 1353 equally spaced \mathbf{q} -points. The black curve represents the ASDM dispersion at 430 K calculated within the phonon quasiparticle picture as in (c). (e) As in (d), but focused around the Γ -point, highlighting the transverse acoustic (TA) and longitudinal acoustic (LA) modes. (f) Phonon density of states computed using the polymorphous structure (orange) and the monomorphous structure with ASDM at 430 K (blue), evaluated with 1353 \mathbf{q} -points. Experimental data (black and grey) at 300, 320, and 200 K are from Refs. [5] and [7]. The calculated PDOS and data from Ref. [7] are scaled by 8 and 4, respectively, to match data from Ref. [5].

across the entire phonon spectrum and reproduces precisely previous measurements of the PDOS [5, 7], without suppressing transverse acoustic phonons. Furthermore, our static DFT calculations for the polymorphous network using the HSE06 and PBE0 functionals [38, 39] revealed a band gap of 0.89 and 1.45 eV, respectively, a significant improvement compared to previous calculations using monomorphous structures or other semi-empirical approaches. Our anharmonic electron-phonon coupling calculations using the polymorphous structure yield a band gap reduction due to the quantum zero-point motion of 35 meV and a further temperature-induced band gap reduction of 212 meV from 0 to 780 K. We also employ the Burstein-Moss shift [56] to account for the heavy p-type doping due to Cu deficiency, and we obtain a band gap widening of 0.26 eV. Taken all contributions together, our values range from 0.8 to 1.7 eV at 300 K, matching experimental values well [1, 43–45].

Our atomistic calculations are based on DFT, with

a combination of semilocal and hybrid functionals. Semilocal DFT calculations are performed in QUANTUM ESPRESSO (QE) [57, 58] using plane wave basis sets and a cutoff of 100 Ry. We employ the Perdew-Burke-Ernzerhof exchange-correlation functional [34] and Optimized Norm-Conserving Vanderbilt pseudopotentials [59]. To obtain polymorphous structures, we employ the ASDM as implemented in the ZG package of the EPW code [60] and the strategy in Refs. [32, 51]. That is, we apply special displacements on the nuclei of the high-symmetry Cu_2Se [e.g. Fig. 1 (a)] along harmonic soft phonons in a supercell and relaxed the system while keeping the lattice constant fixed. This allows the generation of polymorphous structures [Fig. 1(b)], yielding an energy lowering of up to 175 meV per formula unit compared to the monomorphous unit cell (3 atoms). The majority of the calculations are performed on $3 \times 3 \times 3$ supercells using a uniform $3 \times 3 \times 3$ \mathbf{k} -grid, unless stated otherwise. HSE06 and PBE0 calculations are performed

using VASP [61, 62], with a cutoff of 370 eV and the relaxed structures obtained from QE. To evaluate electron and phonon spectral functions of the polymorphous networks, we use electron and phonon band structure unfolding [63] with BANDUP [64, 65] and ZG.x [51], respectively. To account for anharmonic electron-phonon coupling in monomorphous and polymorphous structures, we apply special displacements on the nuclei using temperature-dependent anharmonic phonons computed by the ASDM. Full computational details are available in the supplemental information (SI) [66].

Figure 1(c) shows the phonon dispersions of cubic Cu_2Se obtained within the phonon quasiparticle picture using *symmetrized* interatomic force constants calculated for the polymorphous structure, and the monomorphous structure with and without anharmonic corrections. The harmonic phonon dispersion calculated using the monomorphous structure exhibits large instabilities across the entire reciprocal space. All instabilities in the phonon dispersion are eliminated when the more stable polymorphous structure is employed. Accounting for phonon self-energy corrections at 430 K within the ASDM, the acoustic phonons exhibit a considerable softening, moving lower in energy, while high-energy optical phonons increase in energy. In the SI, we provide the temperature dependence of the phonon dispersion [Fig. S1(a)] and the temperature dependence of the optical phonons at the zone-center, accounting for the longitudinal-transverse optical mode splitting due to long-range effects [Table I and Figs. S1(b), S2 [66]]. The ASDM convergence performance for evaluating anharmonic phonons at 430 K is shown in Figs. S3 and S4 [66].

We then examine the effects of atomic disorder on the vibrational dynamics. In Fig. 1(d), we present the phonon spectral function of polymorphous Cu_2Se obtained by phonon unfolding and without applying the crystal symmetries on the interatomic force constants. Our results reveal strongly overdamped vibrations, deviating from the quasi-particle band theory [monomorphous + ASDM in Fig. 1(d)]. The slow ionic diffusion [7], mimicked by our quasistatic polymorphous network, leads to strongly correlated vibrations with finite lifetimes, suggesting significant phonon-phonon scattering rates that limit thermal conductivity. Examining the low-frequency region around the zone-center [Fig. 1(e)], we find that local disorder preserves transverse acoustic modes, inconsistent with a phonon-liquid picture. To validate the use of the polymorphous structure for describing vibrational properties, we compute the PDOS and compare it with measurements [5, 7], as shown in Fig. 1(f). The PDOS computed for the polymorphous network yields excellent agreement with experiments across the phonon energy range of 0 - 35 meV, exhibiting large broadening without sharp features. In contrast, standard anharmonic approaches using monomorphous cells and accounting for anharmonicity only through

temperature-dependent self-energy corrections [27], result in a narrower frequency range (0 - 25 meV) and sharp peaks not observed in experiments [monomorphous + ASDM in Fig. 1(f)]. Notably, experiments show that the PDOS remains almost unchanged over the temperature range 320 - 900 K [7]. Overall, our results in Fig. 1(f) suggest that local disorder plays a more significant role in capturing anharmonicity in superionic systems than self-energy corrections in monomorphous models derived from higher-order diagrams [28, 32, 69]. The success of using a quasistatic polymorphous network, with atoms localized in one of the potential energy wells, aligns with slow, low-energy hopping relaxations. These localized dynamics minimally disrupt low-energy vibrations, allowing for transverse acoustic phonon propagation despite the extreme anharmonicity, similar to findings for ultrasoft halide perovskites [51, 70].

We next analyze the effects of disorder and phonon anharmonicity on the radial distribution functions (RDFs) [Eq. (1) in SI [66]]. In Fig. 2(a), we report the RDF of Cu-Se bonds calculated using polymorphous structures generated for different supercell sizes without considering thermal effects. In supplemental Fig. S5 [66], we also report Cu-Cu and Se-Se RDFs which compare well with experiments [48] and MD calculations [27]. Unlike the RDF of the monomorphous network, represented by the vertical dashed lines in Fig. 2(a), the RDFs for the polymorphous structures display broad features and indicate a wide distribution of bond lengths, reflecting local structure within the system. Fig. 2(a) and data in supplemental Table II [66] show small differences between the RDFs calculated for different supercell sizes, suggesting that bond length statistics are captured well even by the $2 \times 2 \times 2$ supercell. We also observe that the shortest Cu-Se bond peak position deviates slightly (1.9 % away) from the monomorphous cell value and the experimental value of 2.53 Å at 430 K [48]. Figure 2(b) shows the RDF in the temperature range 300 - 780 K calculated using $3 \times 3 \times 3$ supercells that account for both local and thermal disorder via the ASDM. Anharmonic vibrational dynamics lead to the shift of the first RDF peak, improving agreement between theory and experiment. This highlights the importance of both local and thermal disorder in reproducing structural features. The thermal disorder also leads to a larger broadening and decrease in amplitude of the first RDF peak. For example, the RDF peak calculated for 430 K has a full width at half maximum (FWHM) of 0.7 Å compared to 0.32 Å when no thermal disorder is introduced. The temperature dependence of the first RDF peak position and FWHM are available in the SI Table III [66].

Subsequently, we determine the effects of structural disorder on the temperature-dependent electronic properties. In Fig 2(c) we report our HSE06 calculations for the electron band structure of the monomorphous and spectral function of the polymorphous cubic Cu_2Se . To

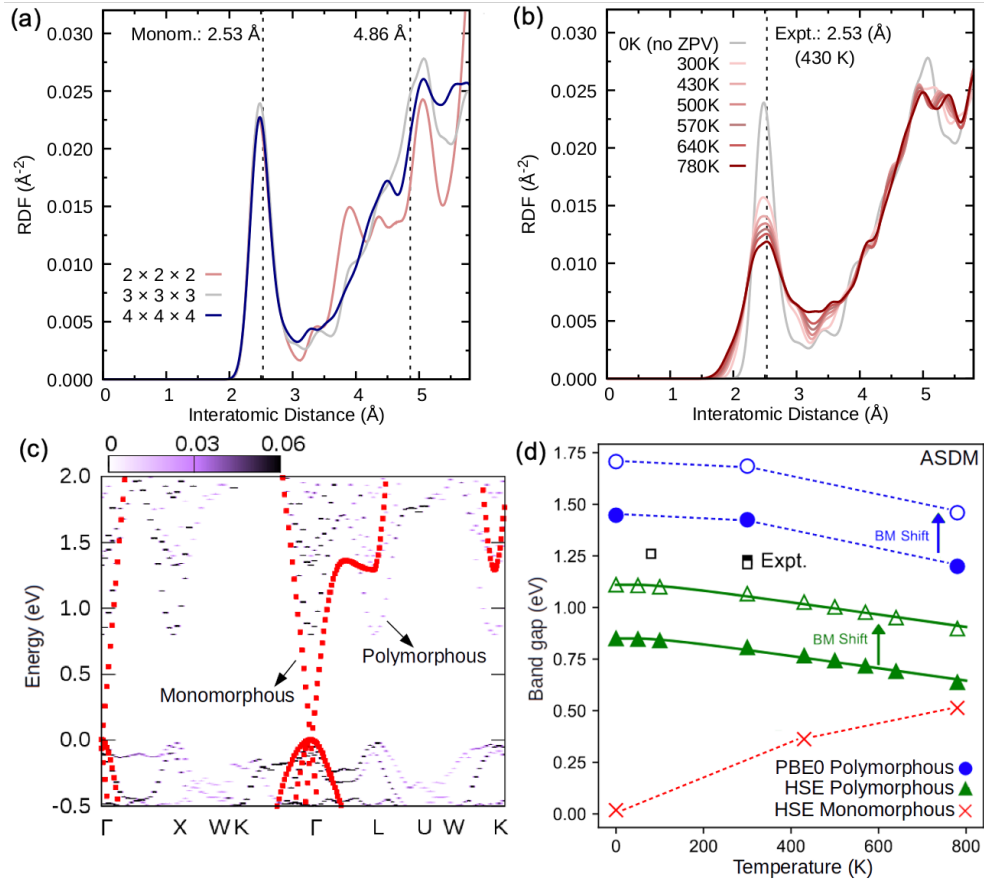


FIG. 2. (a,b) Cu-Se bonding Radial Distribution Function (RDF) calculated with MAISE [67] for (a) $2 \times 2 \times 2$, $3 \times 3 \times 3$, and $4 \times 4 \times 4$ polymorphous supercells at 0 K without zero-point vibrations (ZPV) and (b) $3 \times 3 \times 3$ supercells using the ASDM on top of the polymorphous network to account for thermal disorder, from 300 to 780 K. The experimental value is from Ref. [48]. (c) HSE06 electron spectral function of cubic Cu_2Se calculated using band structure unfolding and the $2 \times 2 \times 2$ polymorphous supercell (colored map). The HSE06 band structure calculated for the monomorphous cell is shown in red. (d) HSE06 (green) and PBE0 (blue) temperature-dependent band gaps calculated for $3 \times 3 \times 3$ polymorphous supercells including anharmonic vibrations. The HSE06 data obtained for the monomorphous structure in $3 \times 3 \times 3$ supercells are shown in red. Green solid lines represent single Einstein oscillator fits (see main text) to the HSE06 data computed for the polymorphous structure. Red and blue dashed lines are used as a guide to the eye. Empty circles and triangles represent Burstein-Moss (BM) shifted data by 0.26 eV. All calculated ASDM data represent the average band gap obtained from an antithetic pair [68]. Experimental values of $\text{Cu}_{1.9}\text{Se}$ (filled square) and Cu_2S (empty squares) are from Refs. [1] and [45].

obtain the spectral function, we simulate positional polymorphism in a $2 \times 2 \times 2$ supercell and perform band unfolding using 149 \mathbf{k} -points. The monomorphous structure yields a semi-metallic behavior, consistent with previous results [35–37]. Allowing for positional polymorphism in a $2 \times 2 \times 2$ supercell of cubic Cu_2Se opens a gap at the Γ -point of 0.82 eV. This value converges within 0.1 eV with our HSE06 band gap calculations of 0.88 and 0.89 eV using the $3 \times 3 \times 3$ and $4 \times 4 \times 4$ supercells, respectively (Fig. S6 [66]). Unlike the vibrational spectral function [Fig. 1(d)], the electron spectral function in Fig. 2(c) exhibits well-defined quasi-particle peaks, consistent with the electronic spectrum of a crystalline semiconductor. Furthermore, symmetry-breaking domains in cubic Cu_2Se create replicas of the band edges near the high-symmetry points X, L, and K, preserving dispersive

bands. This ensures that the effective masses remain optimal for excellent charge transport and thermoelectric performance.

Figure 2(d) shows our HSE06 calculations for the temperature-dependent band gap of monomorphous and polymorphous cubic Cu_2Se , accounting for anharmonic electron-phonon coupling within the ASDM. Our calculations for the monomorphous structure show a band gap widening as the temperature increases, contrary to experimental measurements in Cu-based compounds [45, 71–75]. The decrease in the band gap with temperature, typical for traditional semiconductors [55, 68, 76–81], is captured correctly when we account for positional polymorphism [Fig.2(d)], giving a monotonic band gap decrease of 0.04 eV from 50 to 300 K. This agreement highlights the significant influence of local disorder on

electron-phonon coupling in Cu-based superionic conductors, as previously observed in polymorphous perovskites [51]. We further apply a Bose-Einstein oscillator fit [78] of the form $-\alpha - 2\alpha/(e^{\Theta/T} - 1)$ (green line), and find $\alpha = 35$ meV and $\Theta = 269$ K, which represent the zero-point renormalization and the effective phonon temperature, respectively. From Θ , we extract an effective energy of 23 meV, demonstrating that high-energy optical vibrations dominate band gap renormalization in Cu₂Se. We emphasize that the size of the supercell is critical for capturing electron-phonon coupling effects, as shown in Figs. S6 and S7 [66]. Our data is also well described by the Varshni relation [66, 82] [Fig. S8].

Despite accounting for local disorder and electron-phonon coupling, our HSE06 band gap at 300 K still underestimates experiment [1] by 0.33 eV. To account for the heavy p-type doping due to 5% Cu deficiency in the measured experimental samples [9], we also evaluate the Burstein-Moss (BM) shift [56, 66] due to band filling and Pauli blocking. We assume Cu_{1.9}Se, a three-fold degenerate parabolic band edge with spin degeneracy, and use the experimental hole effective mass [66, 83]. This results in an additional 0.26 eV gap opening for Cu_{1.9}Se [empty triangles in Fig. 2 (d)], further improving the agreement with the experimental value of 1.23 eV [1]. For completeness, in Fig. 2(d), we also report the electron-phonon renormalized band gap at the PBE0 level, which is 1.45 eV at 0 K and 1.43 eV at 300 K. Combined with a BM shift of 0.26 eV (empty circles), these values establish an upper bound to our band gap estimates, consistent with experimental results at room temperature that span a wide range [1, 43, 44, 73–75].

In conclusion, we developed an efficient first-principles framework to simulate strong anharmonicity and electron-phonon coupling in Cu-based superionic conductors without MD simulations. Relying on the ASDM, we demonstrate that quasistatic polymorphous networks of cubic Cu₂Se lead to (i) strongly overdamped vibrational dynamics without suppressing transverse acoustic modes; (ii) an accurate description of the PDOS, supporting the concept that atoms exhibit anharmonic vibrations and disorder, rather than translational diffusion characteristic of a liquid; (iii) well-defined electron band structures; (iv) a large band gap opening compared to the monomorphous structure; and (v) a correct treatment to electron-phonon coupling compared to monomorphous structures, resulting in a decreasing band gap with increasing temperature, consistent with experiments. The present work lays the foundations for systematic first-principles calculations of the thermal conductivity, heat capacity, electrical conductivity, and Seebeck coefficients at finite temperatures, determining the performance of superionic thermoelectrics.

This work is supported by National Science Foundation Award No. 2114424. Computational resources are from National Energy Research Scientific Computing

(NERSC) Center (Contract No. DEAC02-05CH11231) for phonons and Advanced Cyber infrastructure Coordination Ecosystem: Services and Support (ACCESS) award DMR200031 for band structure calculations. M.Z. acknowledges funding by the European Union (project ULTRA-2DPK / HORIZON-MSCA-2022-PF-01 / Grant Agreement No. 101106654). Views and opinions expressed are however those of the authors only and do not necessarily reflect those of the European Union or the European Commission. Neither the European Union nor the granting authority can be held responsible for them. We also acknowledge computational resources from the EuroHPC Joint Undertaking and supercomputer LUMI [https://lumi-supercomputer.eu/], hosted by CSC (Finland) and the LUMI consortium through a EuroHPC Extreme Scale Access call.

* zachariasmaros@gmail.com

† kioup@umich.edu

- [1] G. K. Padam, *Thin Solid Films* **150**, 89 (1987).
- [2] H. Liu, X. Shi, F. Xu, L. Zhang, W. Zhang, L. Chen, Q. Li, C. Uher, T. Day, and G. Snyder Jeffrey, *Nat. Mater.* **11**, 422 (2012).
- [3] F. Liu, M. Huang, Z. Gong, W. Ao, Y. Li, and J. Li, *J. Alloys Compd.* **651**, 648 (2015).
- [4] L. Yang, Z.-G. Chen, G. Han, M. Hong, Y. Zou, and J. Zou, *Nano Energy* **16**, 367 (2015).
- [5] H. Liu, J. Yang, X. Shi, S. A. Danilkin, D. Yu, C. Wang, W. Zhang, and L. Chen, *J. Materiomics.* **2**, 187 (2016).
- [6] T. P. Bailey, S. Hui, H. Xie, A. Olvera, P. F. P. Poudeu, X. Tang, and C. Uher, *J. Mater. Chem. A* **4**, 17225–17235 (2016).
- [7] D. J. Voneshen, H. C. Walker, K. Refson, and J. P. Goff, *Phys. Rev. Lett.* **118**, 145901 (2017).
- [8] A. A. Olvera, N. A. Moroz, P. Sahoo, P. Ren, T. P. Bailey, A. A. Page, C. Uher, and P. F. P. Poudeu, *Energy Environ. Sci.* **10**, 1668–1676 (2017).
- [9] Z. Zhang, K. Zhao, T.-R. Wei, P. Qiu, L. Chen, and X. Shi, *Energy Environ. Sci.* **13**, 3307–3329 (2020).
- [10] H. Hu, Y. Ju, J. Yu, Z. Wang, J. Pei, H.-C. Thong, J.-W. Li, B. Cai, F. Liu, Z. Han, *et al.*, *Nat. Mater.* **23**, 527–534 (2024).
- [11] Y.-X. Zhang, Q.-Y. Huang, X. Yan, C.-Y. Wang, T.-Y. Yang, Z.-Y. Wang, Y.-C. Shi, Q. Shan, J. Feng, and Z.-H. Ge, *Nat. Commun.* **15** (2024).
- [12] W. Liu, H. Wang, L. Wang, X. Wang, G. Joshi, G. Chen, and Z. Ren, *J. Mater. Chem. A* **1**, 13093 (2013).
- [13] X. Yan, B. Poudel, Y. Ma, W. S. Liu, G. Joshi, H. Wang, Y. Lan, D. Wang, G. Chen, and Z. F. Ren, *Nano Lett.* **10**, 3373 (2010).
- [14] R. D. Heyding and R. M. Murray, *Can. J. Chem.* **54**, 841 (1976).
- [15] A. Stevels and F. Jellinek, *Recueil des Travaux Chimiques des Pays-Bas* **90**, 273 (1971).
- [16] W. Borchert, *Z. Kristallogr.* **106**, 5 (1945).
- [17] T. Takahashi, O. Yamamoto, F. Matsuyama, and Y. Noda, *J. Solid State Chem.* **16**, 35–39 (1976).
- [18] H. T. Evans, *Science* **203**, 356–358 (1979).

- [19] Y. G. Asadov, L. V. Rustamova, G. B. Gasimov, K. M. Jafarov, and A. G. Babajev, *Ph. Transit.* **38**, 247–259 (1992).
- [20] L. Gulay, M. Daszkiewicz, O. Strok, and A. Pietraszko, *Chem. Met. Alloys* **4**, 200–205 (2011).
- [21] N. Roth and B. B. Iversen, *Acta Crystallogr. Section A* **75**, 465 (2019).
- [22] S. Kavirajan, S. Harish, J. Archana, M. Shimomura, and M. Navaneethan, *Mater. Lett.* **298**, 129957 (2021).
- [23] P. K. Jain, *J. Phys. Chem. C* **127**, 18253–18255 (2023).
- [24] H. Kim, S. Ballikaya, H. Chi, J.-P. Ahn, K. Ahn, C. Uher, and M. Kaviany, *Acta Mater.* **86**, 247 (2015).
- [25] S. Namsani, S. Auluck, and J. K. Singh, *Appl. Phys. Lett.* **111**, 163903 (2017).
- [26] K. Zhuo, J. Wang, J. Gao, U. Landman, and M.-Y. Chou, *Phys. Rev. B* **102**, 064201 (2020).
- [27] W. Zhang, C. Zheng, Y. Dong, J.-Y. Yang, and L. Liu, *Phys. Chem. Chem. Phys.* **22**, 28086 (2020).
- [28] T. Tadano and S. Tsuneyuki, *Phys. Rev. B* **92**, 054301 (2015).
- [29] D. Hooton, *London Edinburgh Philos. Mag. & J. Sci.* **46**, 422 (1955).
- [30] O. Hellman, P. Steneteg, I. A. Abrikosov, and S. I. Simak, *Phys. Rev. B* **87**, 104111 (2013).
- [31] I. Errea, M. Calandra, and F. Mauri, *Phys. Rev. B* **89**, 064302 (2014).
- [32] M. Zacharias, G. Volonakis, F. Giustino, and J. Even, *Phys. Rev. B* **108**, 035155 (2023).
- [33] J. P. Perdew and Y. Wang, *Phys. Rev. B* **45**, 13244 (1992).
- [34] J. P. Perdew, K. Burke, and M. Ernzerhof, *Phys. Rev. Lett.* **77**, 3865 (1996).
- [35] M. Råsander, L. Bergqvist, and A. Delin, *J. Phys. Condens. Matter* **25**, 1 (2013).
- [36] K. Tyagi, B. Gahtori, S. Bathula, S. Auluck, and A. Dhar, *Appl. Phys. Lett.* **105** (2014).
- [37] Y. Zhang, Y. Wang, L. Xi, R. Qiu, X. Shi, P. Zhang, and W. Zhang, *J. Chem. Phys.* **140** (2014).
- [38] A. V. Krukau, O. A. Vydrov, A. F. Izmaylov, and G. E. Scuseria, *J. Chem. Phys.* **125**, 224106 (2006).
- [39] Y.-i. Matsushita, K. Nakamura, and A. Oshiyama, *Phys. Rev. B* **84**, 075205 (2011).
- [40] F. Tran and P. Blaha, *Phys. Rev. Lett.* **102**, 226401 (2009).
- [41] D. Koller, F. Tran, and P. Blaha, *Phys. Rev. B* **83**, 195134 (2011).
- [42] Y. Sun, L. Xi, J. Yang, L. Wu, X. Shi, L. Chen, J. Snyder, J. Yang, and W. Zhang, *J. Mater. Chem. A* **5**, 5098 (2017).
- [43] S. A. Gad, H. Shaban, H. A. Saleh, and T. A. Hameed, *JSS* **11**, 113009 (2022).
- [44] G. P. Sorokin, Y. M. Papshev, and O. P. T., *Sov. Phys. Solid State* **7**, 1810 (1966).
- [45] R. Marshall and S. S. Mitra, *J. Appl. Phys.* **36**, 3882–3883 (1965).
- [46] P. Lukashev, W. R. L. Lambrecht, T. Kotani, and M. van Schilfgaarde, *Phys. Rev. B* **76**, 195202 (2007).
- [47] J. M. Klan, D. K. Harper, J. P. Ruffley, X. Y. Gan, J. E. Millstone, and J. K. Johnson, *J. Phys. Chem. C* **125**, 12324 (2021).
- [48] S. Danilkin, M. Avdeev, T. Sakuma, R. Macquart, and C. Ling, *J. Alloys Compd.* **509**, 5460 (2011).
- [49] S. A. Danilkin, A. N. Skomorokhov, A. Hoser, H. Fuess, V. Rajevac, and N. N. Bickulova, *J. Alloys Compd.* **361**, 57 (2003).
- [50] A. Skomorokhov, D. Trots, M. Knapp, N. Bickulova, and H. Fuess, *J. Alloys Compd.* **421**, 64 (2006).
- [51] M. Zacharias, G. Volonakis, F. Giustino, and J. Even, *npj Comput. Mater.* **9**, 153 (2023).
- [52] X. G. Zhao, G. M. Dalpian, Z. Wang, and A. Zunger, *Phys. Rev. B* **101**, 1 (2020).
- [53] X.-G. Zhao, O. I. Malyi, and A. Zunger, *Phys. Rev. Mater.* **8**, 125403 (2024).
- [54] G. Trimarchi, Z. Wang, and A. Zunger, *Phys. Rev. B* **97**, 035107 (2018).
- [55] M. Zacharias and F. Giustino, *Phys. Rev. Res.* **2**, 7 (2020).
- [56] E. Burstein, *Phys. Rev.* **93**, 632 (1954).
- [57] P. Giannozzi, O. Andreussi, T. Brumme, O. Bunau, M. Buongiorno Nardelli, M. Calandra, R. Car, C. Cavazzoni, D. Ceresoli, M. Cococcioni, *et al.*, *J. Phys. Condens. Matter* **29**, 465901 (2017).
- [58] P. Giannozzi, O. Baseggio, P. Bonfà, D. Brunato, R. Car, I. Carnimeo, C. Cavazzoni, S. de Gironcoli, P. Delugas, F. Ferrari Ruffino, *et al.*, *J. Phys. Condens. Matter* **21**, 395502 (2009).
- [59] D. R. Hamann, *Phys. Rev. B* **88**, 85117 (2013).
- [60] H. Lee, S. Poncé, K. Bushick, S. Hajinazar, J. Lafuente-Bartolome, J. Leveillee, C. Lian, F. Macheda, H. Paudyal, W. H. Sio, *et al.*, *npj Comput. Mater.* **9**, 156 (2023).
- [61] P. E. Blöchl, *Phys. Rev. B* **50**, 17953 (1994).
- [62] G. Kresse and J. Furthmüller, *Comput. Mater. Sci.* **6**, 15 (1996).
- [63] P. B. Allen, T. Berlijn, D. A. Casavant, and J. M. Soler, *Phys. Rev. B* **87**, 085322 (2013).
- [64] P. V. Medeiros, S. Stafström, and J. Björk, *Phys. Rev. B* **89** (2014).
- [65] P. V. C. Medeiros, S. S. Tsirkin, S. Stafström, and J. Björk, *Phys. Rev. B* **91**, 041116 (2015).
- [66] Full methodology details, supplemental Figs. S1-S8 and Tables I-III.
- [67] W. Ibarra-Hernández, S. Hajinazar, G. Avendaño-Franco, A. Bautista-Hernández, A. N. Kolmogorov, and A. H. Romero, *Phys. Chem. Chem. Phys.* **20**, 27545 (2018).
- [68] M. Zacharias and F. Giustino, *Phys. Rev. B* **94**, 075125 (2016).
- [69] R. Bianco, I. Errea, L. Paulatto, M. Calandra, and F. Mauri, *Phys. Rev. B* **96**, 014111 (2017).
- [70] A. C. Ferreira, S. Paofai, A. Létoublon, J. Ollivier, S. Raymond, B. Hehlen, B. Rufflé, S. Cordier, C. Katan, J. Even, and P. Bourges, *Commun. Phys.* **3** (2020).
- [71] S. Choi, T. Kim, S. Hwang, J. Li, C. Persson, Y. Kim, S.-H. Wei, and I. Repins, *Sol. Energy Mater. Sol. Cells* **130**, 375–379 (2014).
- [72] M. Birkett, C. N. Savory, M. K. Rajpalke, W. M. Linhart, T. J. Whittles, J. T. Gibbon, A. W. Welch, I. Z. Mitrovic, A. Zakutayev, D. O. Scanlon, and T. D. Veal, *APL Mater.* **6** (2018).
- [73] A. Qasrawi and O. A. Omareya, *J. Alloys Compd.* **785**, 1160.
- [74] S. M. Ali, H. K. Hassun, A. A. Salih, R. H. Athab, B. K. H. Al-Maiyaly, and B. H. Hussein, *Chalcogenide Lett.* **19**, 663.
- [75] J. Henry, T. Daniel, V. Balasubramanian, K. Mohanraj, and G. Sivakumar, *Inorg. Nano-Metal Chem.* **51**, 38.
- [76] P. B. Allen and V. Heine, *J. Phys. C: Solid State Phys.*

- 9**, 2305–2312 (1976).
- [77] P. B. Allen and M. Cardona, *Phys. Rev. B* **23**, 1495 (1981).
- [78] F. Giustino, S. G. Louie, and M. L. Cohen, *Phys. Rev. Lett.* **105**, 265501 (2010).
- [79] S. Poncé, Y. Gillet, J. Laflamme Janssen, A. Marini, M. Verstraete, and X. Gonze, *J. Chem. Phys.* **143** (2015).
- [80] A. Miglio, V. Brousseau-Couture, E. Godbout, G. Anto-
nius, Y.-H. Chan, S. G. Louie, M. Côté, M. Giantomassi,
and X. Gonze, *npj Comput. Mater.* **6** (2020).
- [81] M. Engel, H. Miranda, L. Chaput, A. Togo, C. Verdi,
M. Marsman, and G. Kresse, *Phys. Rev. B* **106**, 094316
(2022).
- [82] Y. Varshni, *Physica* **34**, 149 (1967).
- [83] Voskanyan, A. A., Inglizyan, P. N., Lalykin, S. P.,
Plyutto, I. A., and Shevchenko, Ya. M., *Fiz. Tekh.
Poluprovodn* **12** (1978).